

An estimation of the $^{18}\text{O}/^{16}\text{O}$ ratio of UT/LMS ozone based on artefact CO in air sampled during CARIBIC flights

S. Gromov¹, C. A. M. Brenninkmeijer¹

¹ Max Planck Institute for Chemistry, Mainz, Germany

Correspondence to: S. Gromov (sergey.gromov@mpic.de)

Abstract

An issue of O₃-driven artefact production of CO in the UT/LMS air analysed in the CARIBIC-1 project is being discussed. By confronting the CO mixing/isotope ratios obtained from different analytical instrumentation, we (i) Reject natural/artificial sampling and mixing effects as possible culprits of the problem, (ii) Ascertain the photochemical nature and quantify the strength of the effect in a general contamination kinetic framework, and (iii) Demonstrate the successful application of the isotope mass-balance calculations for inferring the isotope signature of the contamination source. The $^{18}\text{O}/^{16}\text{O}$ ratios of the latter unambiguously indicate the oxygen being inherited from O₃. The $^{13}\text{C}/^{12}\text{C}$ ratios hint at reactions of trace amounts of organics with ample stratospheric O₃ that could have yielded the artificial CO. While the exact contamination mechanism is not known, it is clear that the issue pertains only to the earlier (first) phase of the CARIBIC project. Finally, estimated UT/LMS ozone $^{18}\text{O}/^{16}\text{O}$ ratios are lower than those observed in the LMS within the same temperature range, suggesting that higher pressures (240–270 hPa) imply lower isotope fractionation controlling the local $\delta^{18}\text{O}(\text{O}_3)$ value.

1 Introduction

[1] Successful determination of the atmospheric carbon monoxide (CO) content based on the collection of air samples depends on the preservation of the mixing ratio of CO inside the receptacle, from the point of sampling to the moment of physiochemical analysis in a laboratory. A well known example in our field of research is the filling of pairs of glass flasks at South Pole

20 Station for analysis at NOAA in Boulder, Colorado, USA (Novelli *et al.*, 1998). There, the du-
21 plicate air sampling allowed for a degree of quality control which in view of the long transit
22 times, especially during polar winter, was a perhaps not perfect, but certainly a practical meas-
23 ure. Here we deal with a different case: Using aircraft-based collection of very large air samples
24 rendered duplicate sampling unpractical, yet analyses could be performed soon after the sam-
25 pling had taken place because of the proximity of the aircraft's landing location to the labora-
26 tory involved. A presumption of the analytical integrity of the process was that the growth of
27 CO in receptacles is gradual and takes its time. Reminding Thomas Henry Huxley's statement,
28 "The great tragedy of Science – the slaying of a beautiful hypothesis by an ugly fact", it turned
29 out, however, that for air we collected in stainless steel tanks in the upper tropo-
30 sphere/lowermost stratosphere (UT/LMS) higher CO values were measured in the laboratory
31 than measured *in situ* during the collection of these air samples. Moreover, measurement of the
32 stable oxygen isotopic composition of CO from these tanks revealed additional isotopic enrich-
33 ments in ^{18}O of 10‰ or more. It was soon realised that this phenomenon was due to the forma-
34 tion of CO in these tanks and/or possibly in the sampling system and inlet tubing used, by reac-
35 tions involving ozone (Brenninkmeijer *et al.*, 1999).

36 [2] Unexpectedly high $^{18}\text{O}/^{16}\text{O}$ ratios in stratospheric ozone (O_3) were discovered by Konrad
37 Mauersberger using a balloon-borne mass spectrometer (Mauersberger, 1981), which has trig-
38 gered a series of theoretical and experimental studies on atmospheric O_3 heavy isotope enrich-
39 ments (see, *e.g.*, Schinke *et al.* (2006) for a review). In view of the advances in theoretical and
40 laboratory studies on the isotopic composition of O_3 atmospheric measurements are welcome,
41 they do however form a challenge. In the stratosphere O_3 is abundant, but the remoteness of the
42 sampling domain is a problem. In the troposphere, low O_3 concentrations are the main obstacle,
43 as indicated by few experiments performed to date (Krankowsky *et al.*, 1995; Johnston and
44 Thiemens, 1997; Vicars and Savarino, 2014). Nevertheless, recent analytical improvements,
45 namely the use of an indirect method of reacting atmospheric O_3 with a substrate that can be
46 analysed for the isotopic composition of the O_3 -derived oxygen (Vicars *et al.*, 2012), has greatly
47 improved our ability to obtain information on the O_3 isotopic composition.

48 [3] Although the increase of CO concentrations in air stored in vessels is a well recognised
49 problem, to our knowledge a specific O_3 -related process has not been reported yet. Here we dis-
50 cuss this phenomenon and turn its disadvantage into an advantage, namely that of obtaining a
51 valid estimate of the oxygen isotopic composition of O_3 in the UT/LMS, an atmospheric do-
52 main not yet covered by specific measurements. The air samples we examine in this study were

53 collected onboard a passenger aircraft carrying an airfreight container with analytical and
54 air/aerosol sampling equipment on long distance flights from Germany to South India and the
55 Caribbean within the framework of the CARIBIC project (Civil Aircraft for the Regular Inves-
56 tigation of the atmosphere Based on an Instrument Container, [http://www.caribic-](http://www.caribic-atmospheric.com)
57 [atmospheric.com](http://www.caribic-atmospheric.com)).

58 2 Experimental and results

2.1 Whole air sampling

59 [4] CARIBIC-1 (Phase #1, abbreviated hereafter “C1”) was operational from November 1998
60 until April 2002 using a *Boeing 767-300 ER* operated by LTU International Airlines
61 (Brenninkmeijer *et al.*, 1999). Using a whole air sample (WAS) collection system, twelve air
62 samples were collected per flight (of ~10 hours duration at cruise altitudes of 10–12 km) in
63 stainless steel tanks for subsequent laboratory analysis of the abundances of various trace gases,
64 including ^{14}CO . Large air samples were required in view of the ultra-low abundance of this
65 mainly cosmogenic tracer ($10\text{--}100$ molecules cm^{-3} STP, about 40–400 amol/mol). Each C1
66 WAS sample (holding ~350 litres of air STP) was collected within 15–20 min intervals repre-
67 senting the integral of the compositions encountered along flight segments of ~250 km. The
68 overall uncertainty of the measured WAS [CO] is less than $\pm 1\%$ for the mixing ratio and
69 $\pm 0.1\text{‰}/\pm 0.2\text{‰}$ for $\delta^{13}\text{C}(\text{CO})/\delta^{18}\text{O}(\text{CO})$, respectively (Brenninkmeijer, 1993;
70 Brenninkmeijer *et al.*, 2001). Isotope compositions are reported throughout this manuscript us-
71 ing $\delta^i = ({}^iR/{}^iR_{\text{st}} - 1)$ relating the ratio of rare over abundant isotopes iR of interest (i denotes ^{13}C ,
72 ^{18}O or ^{17}O) to the standard ratio ${}^iR_{\text{st}}$. These are V-SMOW of 2005.20×10^{-6} for $^{18}\text{O}/^{16}\text{O}$
73 (Gonfiantini, 1978; Coplen, 1994) and 386.72×10^{-6} for $^{17}\text{O}/^{16}\text{O}$ (Assonov and Brenninkmei-
74 jer, 2003), and V-PDB of 11237.2×10^{-6} for $^{13}\text{C}/^{12}\text{C}$ (Craig, 1957), respectively. As we mention
75 above, the oxygen isotopic composition of the CO present in these WAS samples was cor-
76 rupted, in particular when O_3 levels were as high as 100–600 nmol/mol.

77 [5] CARIBIC-2 (Phase #2, referred to as “C2”) started operation in December 2004 with a Luf-
78 thansa *Airbus A340-600* fitted with a new inlet system and air sampling lines, including PFA
79 lined tubing for trace gas intake (Brenninkmeijer *et al.*, 2007). No flask CO mixing/isotope ratio
80 measurements are performed in C2.

2.2 On-line instrumentation

81 [6] In addition to the WAS collection systems, both C1 and C2 measurement setups include dif-
82 ferent instrumentation for on-line detection of [CO] and [O₃] (hereinafter the squared brackets
83 [] denote the abundance, *i.e.* concentration or mixing ratio, of the respective species). *In situ* CO
84 analysis in C1 is done using a gas chromatography (GC)-reducing gas analyser which provides
85 measurements each 130 s with uncertainty of ± 3 nmol/mol (Zahn *et al.*, 2000). In C2, a vacuum
86 ultraviolet fluorescence (VUV) instrument with lower measurement uncertainty and higher
87 temporal resolution of ± 2 nmol/mol in ~ 2 s (Scharffe *et al.*, 2012) is employed, respectively.
88 Furthermore, the detection frequency for O₃ mixing ratios has also increased, *viz.* from 0.06 Hz
89 in C1 to 5 Hz in C2 (Zahn *et al.*, 2002; Zahn *et al.*, 2012).

2.3 Results

90 [7] When comparing the CO abundances in relation to O₃ mixing ratios for C1 and C2, differ-
91 ences are apparent in the LMS, where C2 CO values are systematically lower. This is illustrated
92 in Figure 1 (a) which presents the LMS CO-O₃ distribution of the C2 measurements overlaid
93 with the C1 *in situ* and WAS data. For the *in situ* CO datasets we calculated the statistics (*ibid.*,
94 Panel (b)) of the samples with respective O₃ abundances clustered in 20 nmol/mol bins, *i.e.* the
95 median and spread of [CO] as a function of [O₃] analysed. (The interquartile range, IQR, is used
96 in the current analysis as a robust measure of the data spread instead of the standard deviation.)
97 The data exhibit large [CO] variations at [O₃] below 400 nmol/mol that primarily reflect pro-
98 nounced seasonal variations in the NH tropospheric CO abundance. With O₃ rising, [CO] in-
99 creasingly becomes stratospheric, and its spread reduces to mere 3.5 nmol/mol and less, as [O₃]
100 surpasses 500 nmol/mol. Despite the comparable spread in C1 and C2 [CO], from
101 400 nmol/mol of [O₃] onwards the C1 CO mixing ratios start to level off, with no samples be-
102 low 35 nmol/mol having been detected, whereas the C2 levels continuously decline. By the
103 580 nmol/mol O₃ bin, C1 [CO] of $39.7_{-1.3}^{+0.7}$ nmol/mol accommodates some extra 15 nmol/mol
104 compared to $25.6_{-1.1}^{+1.2}$ nmol/mol typical for C2 values. Overall, at [O₃] above 400 nmol/mol the
105 conspicuously high [CO] is marked in about 200 *in situ* C1 samples, of which 158 and 69
106 emerge as statistically significant mild and extreme outliers, respectively, when compared
107 against the ample ($n \sim 3 \cdot 10^5$) C2 statistics. (The conventions here follow Natrella (2003),
108 *i.e.* ± 1.5 and ± 3 IQR ranges define the inner and outer statistical fences (ranges outside which
109 the data points are considered mild and extreme outliers) of the C2 [CO] distribution in every
110 O₃ bin, respectively; the statistics include the samples in bins with average [O₃] of

111 420–620 nmol/mol.) None of C1 CO at $[O_3]$ above 560 nmol/mol agrees with the C2 observa-
112 tions. Because the CO levels cannot have changed over the period in question by the difference
113 we find (up to 55%), artefacts and calibration issues need to be scrutinised.

114 [8] Unnatural elevations in the $^{18}O/^{16}O$ ratios of CO from WAS measurements are also evident,
115 as shown in Fig. 2. The large $\delta^{18}O(CO)$ departures that reach beyond +16‰ are found to be
116 proportional to the concomitant O_3 abundances (denoted with colour) and more prominent at
117 lower $[CO]$ (see also Fig. S2 in the Supplementary Material). A rather different relationship,
118 however, is expected from our knowledge of UT/LMS CO sources (plus their isotope signa-
119 tures) and available *in situ* observations (*ibid.*, shown with triangles), as elucidated by
120 Brenninkmeijer *et al.* (1996) (hereafter denoted as “B96”). That is, the more stratospheric CO
121 is, the greater fraction of its local inventory is refilled with the photochemical component
122 stemming from methane oxidation with a characteristic $\delta^{18}O$ signature of $\sim 0\%$ or lower
123 (Brenninkmeijer and Röckmann, 1997). This occurs because the CO sink at ruling UT/LMS
124 temperatures proceeds more readily than its production, as the reaction of hydroxyl radical
125 (OH) with CO, being primarily pressure-dependent, outcompetes the temperature-sensitive re-
126 action of OH with CH_4 . Furthermore, as the lifetime of CO quickly decreases with altitude,
127 transport-mixing effects take the lead in determining the vertical distributions of $[CO]$ and
128 $\delta^{18}O(CO)$ above the tropopause, hence their mutual relationship. This is seen from the B96 data
129 at $[CO]$ below 50 nmol/mol that line-up in a near linear relationship towards the end-members
130 with lowest $^{18}O/^{16}O$ ratios. These result from the largest share of the ^{18}O -depleted photochemi-
131 cal component and extra depletion caused by the preferential removal of $C^{18}O$ in reaction with
132 OH (fractionation about $\sim 11\%$ at pressures below 300 hPa, Stevens *et al.*, 1980;
133 Röckmann *et al.*, 1998b).

134 [9] It is beyond doubt that the enhancements of C1 $C^{18}O$ originate from O_3 , whose large en-
135 richment in heavy oxygen (above +60‰ in $\delta^{18}O$, Brenninkmeijer *et al.*, 2003) is typical and
136 found transferred to other atmospheric compounds (see Savarino and Morin (2012) for a re-
137 view). In Fig. 2 it is also notable that not only the LMS compositions are affected but elevations
138 of (3–10)‰ from the bulk $\delta^{18}O(CO)$ values are present in more tropospheric samples with $[CO]$
139 of up to ~ 100 nmol/mol. These result from the dilution of the least affected tropospheric air
140 with high mixing ratios by CO-poor, however substantially contaminated, stratospheric air,
141 sampled into the same WAS tank. Such sampling-induced mixing renders an unambiguous de-
142 termination of the artefact source’ isotope signature rather difficult, because neither mixing nor
143 isotope ratios of the admixed air portions are known sufficiently well (see below).

144 [10] Differences between the WAS and *in situ* measured [CO] – a possible indication that the
145 $\delta^{18}\text{O}(\text{CO})$ contamination pertains specifically to the WAS data – average at $\bar{\Delta}_{\text{WAS-}in\ situ} =$
146 5.3 ± 0.2 nmol/mol (1 SD of the mean, $n = 408$) and happen to be random with respect to any op-
147 erational parameter or measured characteristic in C1, *i.e.* irrespective of CO or O₃ abundances.
148 The quoted mixing ratio discrepancy remained after several calibrations between the two sys-
149 tems had been performed, and likely results from the differences in the detection methods, drifts
150 of the calibration standards used (see details in Brenninkmeijer *et al.*, 2001) and a short-term
151 production of CO in the stainless steel tanks during sampling. The large spread of $\Delta_{\text{WAS-}in\ situ}$
152 of ± 3.5 nmol/mol (1σ of the population) ensues from the fact that the *in situ* sampled air corre-
153 sponds to (2–4)% of the concomitantly sampled WAS volume, as typically 6–7 *in situ* collec-
154 tions of ~ 5 s were made throughout one tank collection of 17–21 min. The integrity of the WAS
155 CO is further affirmed by the unsystematic distribution of the artefact compositions among
156 tanks (an opposite case for $\delta^{18}\text{O}(\text{CO}_2)$ in C1 is discussed by Assonov *et al.*, 2009). Overall, the
157 WAS and *in situ* measured CO mixing ratios correlate extremely well (adj. $R^2 = 0.972$, slope of
158 0.992 ± 0.008 (1σ), $n = 408$). However, both anomalies in [CO] and $\delta^{18}\text{O}(\text{CO})$ manifest clear but
159 complex functions of the concomitant [O₃]. That is, the C1 *in situ* and WAS data very likely
160 evidence artefacts pertaining to the O₃-driven effect of the same nature. Below we ascertain and
161 quantify these.

162 3 Discussion

163 [11] Three factors may lead to the (artefact) distributions such as seen for C1 *in situ* [CO] at the
164 LMS O₃ abundances, namely:

165 [12] (i) Strong (linear) natural mixing, such as enhanced stratosphere-troposphere exchange
166 (STE), when a [CO] outside the statistically expected range results from the integration of air
167 having dissimilar ratios of the tracers' abundances, *viz.* $\rho_{\text{O}_3:\text{CO}} = [\text{O}_3]/[\text{CO}]$. For example, mixing
168 of two air parcels in a 15%:85% proportion (by moles of air) with typical $\rho_{\text{O}_3:\text{CO}}$ of 700:24
169 (stratospheric) and 60:125 (tropospheric), respectively, yields an integrated composition with
170 $\rho_{\text{O}_3:\text{CO}}$ of $\sim 580:40$ which indeed corresponds to C1 data (this case is exemplified by the mixing
171 curve in Fig. 1). Nonetheless, occurrences of rather high (compared to the typical
172 24–26 nmol/mol) stratospheric CO mixing ratios (in our case, ~ 40 nmol/mol at the concomitant
173 [O₃] of 500–600 nmol/mol) are rare. For instance, a deep STE similar to that described by
174 Pan *et al.* (2004) was observed by C2 only once (*cf.* the outliers at [O₃] of 500 nmol/mol in
175 Fig. 1), whereas the C1 outliers were exclusively registered in some 12 flights during

176 1997–2001. No relation between these outliers and the large-scale [CO] perturbation due to ex-
177 tensive biomass burning in 1997/1998 (Novelli *et al.*, 2003) is established, otherwise elevated
178 CO mixing ratios should manifest themselves at lower [O₃] as well. Other tracers detected in
179 CARIBIC provide supporting evidence against such strongly STE-mixed air having been cap-
180 tured by C1. That is, the binned distributions for the water vapour and de-trended N₂O (similar
181 to that for [CO] vs. [O₃] presented in Fig. 1, not shown here) are greatly similar in C1 and C2.
182 Whereas the small relative variations in atmospheric [N₂O] merely confirm matching [O₃] sta-
183 tistics in CARIBIC, the stratospheric [H₂O] distributions witness no $\rho_{\text{O}_3:\text{H}_2\text{O}}$ values correspond-
184 ing to the C1 outliers' $\rho_{\text{O}_3:\text{CO}}$, suggesting the latter being unnaturally low.

185 [13] (ii) Mixing effects can also occur artificially, originating from sampling peculiarities or data
186 processing. Since the CARIBIC platform is not stationary, about 5 s long sampling of an *in situ*
187 air probe in C1 implies integration of the compositions encountered along some hundred met-
188 res, owing to the high aircraft speed. This distance may cover a transect between tropospheric
189 and stratospheric filaments of much different compositions. The effect of such ‘translational
190 mixing’ can be simulated by averaging the sampling data with higher temporal frequency over
191 longer time intervals. In this respect, the substantially more frequent CO data in C2 (<1 s) were
192 artificially averaged over a set of increasing intervals to reckon whether the long sampling pe-
193 riod in C1 could be the culprit for skewing its CO–O₃ distribution. As a result, the original C2
194 data and their averages (equivalent to the C1 CO sample injection time) differ negligibly, as do
195 the respective $\rho_{\text{O}_3:\text{CO}}$ values; the actual C2 CO–O₃ statistic in the region of interest ([O₃] of
196 540–620 nmol/mol) remains insensitive to integration of up to 300 s. Furthermore, a very
197 strong artificial mixing with an averaging interval of at least 1200 s (comparable to C1 WAS
198 sampling time) is required to yield the averages from the C2 data with $\rho_{\text{O}_3:\text{CO}}$ characteristic for
199 the C1 outliers.

200 [14] (iii) In view of the above, it is unlikely that any natural or artificial mixing processes are in-
201 volved in the stratospheric [CO] discrepancies seen in C1. It therefore stands to reason to con-
202 clude that the sample contamination in C1 occurred prior the probed air reaching the analyti-
203 cal/sampling instrumentation in the container, since clearly elevated stratospheric CO mixing
204 ratios are common to WAS and *in situ* data. Two more indications, *viz.* growing [CO] discrep-
205 ancy with increasing O₃ abundance, and the strong concomitant signal in $\delta^{18}\text{O}(\text{CO})$, imply that
206 O₃-mediated photochemical production of CO took place. Further, by confronting the C1 and
207 C2 [CO] measurements in a kinetic framework (detailed in Appendix A), we quantify the arte-
208 fact CO component being chiefly a function of O₃ abundance as

$$C_c = b \cdot [\text{O}_3]^2, b = (5.19 \pm 0.12) \cdot 10^{-5} \text{ [mol/nmol]}, \quad (1)$$

209 which is equivalent to 8–18 nmol/mol throughout the respective $[\text{O}_3]$ range of
 210 400–620 nmol/mol (see Fig. 1 (d)). Subtracting this artefact signal yields the corrected *in situ*
 211 C1 CO–O₃ distribution conform to that of C2 (*cf.* red symbols in Fig. 1 (a)).

212 [15] Importantly, since we can quantify the contamination strength using only the O₃ abundance,
 213 the continuous *in situ* C1 $[\text{O}_3]$ data allows to estimate the integral artefact CO component in
 214 each WAS sample and, if the isotope ratio of contaminating O₃ is known, to derive the initial
 215 $\delta^{18}\text{O}(\text{CO})$. The latter, as it was mentioned above, is subject to strong sample-mixing effects,
 216 which is witnessed by $\delta^{18}\text{O}(\text{CO})$ outliers even at relatively high $[\text{CO}]$ up to 100 nmol/mol. Ac-
 217 counting for such cases is, however, problematic since it is necessary to distinguish the propor-
 218 tions of the least modified (tropospheric) and significantly affected (stratospheric) components
 219 in the resultant WAS sample mix. In reality, however, this information is not available, there-
 220 fore we applied an *ad hoc* correction approach (which is capable of determining the contamina-
 221 tion source (*i.e.*, O₃) isotope signature as well), as described in the following.

3.1 Contamination isotope signatures

222 [16] Practically we resort to the differential mixing model (MM, originally known as the “Keel-
 223 ing-plot”), because it requires only the estimate of the artefact component mixing ratio, but no
 224 assumptions on the (unknown) shares and isotope signatures of the air portions mixed in a given
 225 WAS tank. The MM parameterises the admixing of the portion of artefact CO to the WAS sam-
 226 ple with the “true” initial composition, as formulated below:

$$\begin{cases} {}^i\delta_a C_a = C_t {}^i\delta_t + C_c {}^i\delta_c \\ C_t \equiv (C_a - C_c) \end{cases}, \quad (0)$$

227 where indices a , c and t distinguish the abundances C and isotope compositions ${}^i\delta$ (i may refer
 228 to ¹³C or ¹⁸O) pertaining to the analysed sample, estimated contamination and “true” composi-
 229 tion sought (*i.e.*, C_t and ${}^i\delta_t$), respectively. (Here the contamination strength C_c is derived by in-
 230 tegrating Eq. (1) using the *in situ* C1 $[\text{O}_3]$ data for each WAS sample.) By rewriting the above
 231 equation w.r.t. the isotope signature of the admixed portion ${}^i\delta_c$, one obtains:

$${}^i\delta_c = {}^i\delta_t + ({}^i\delta_a - {}^i\delta_t)(1 + C_t/C_c), \quad (2)$$

232 which signifies that linear regression of the measured ${}^i\delta_a$ as a function of the reciprocal of C_c
 233 yields the estimated contamination signature ${}^i\delta_c$ at $(C_c)^{-1} \rightarrow 0$. (The Keeling plot detailing the
 234 calculations with the MM is shown in Supplementary Material, Fig. S3.) The MM described by

235 Eq. (2) provides adequate results only for the invariable initial compositions ($C_i, {}^i\delta_i$), therefore
236 we apply it to the subsets of samples picked according to the same reckoned C_i (within a
237 ± 2 nmol/mol window, $n > 7$). Such selection, however, may be insufficient: Due to the strong
238 sampling effects in the WAS samples (see previous Section), it is possible to encounter samples
239 that integrate different air masses to the same C_i but rather different average ${}^i\delta_i$. The solution in
240 this case is to refer to the goodness of the MM regression fit, because the R^2 intrinsically meas-
241 ures the linearity of the regressed data, *i.e.* closeness of the “true” values in a regarded subset of
242 samples, irrespective of underlying reasons for that.

243 [17] Higher R^2 values thus imply higher consistency of the estimate, as demonstrated in Fig. 3
244 showing the calculated ${}^i\delta_c$ for C_i below 80 nmol/mol as a function of the regression R^2 . The latter
245 decreases with greater C_i (*i.e.*, larger sample subset size, since tropospheric air is more often
246 encountered) and, conformably, larger variations in ${}^i\delta_i$. Ultimately, at lower R^2 the inferred ${}^{18}\text{O}$
247 signatures converge to values slightly above zero expected for uncorrelated data, *i.e.* C1
248 $\delta^{18}\text{O}(\text{CO})$ tropospheric average. A similar relationship is seen for the ${}^{13}\text{C}$ signatures (they con-
249 verge around -28‰), however, there are no consistent estimates found (R^2 is generally below
250 0.4). Since such is not the case for $\delta^{18}\text{O}$, the MM is not sufficiently sensitive to the changes
251 caused by the contamination, which implies that the artefact CO $\delta^{13}\text{C}$ should be within the
252 range of the “true” $\delta^{13}\text{C}(\text{CO})$ values. Interestingly, the MM is rather responsive to the growing
253 fraction of the CH_4 -derived component in CO with increasing $[\text{O}_3]$, as the ${}^{13}\text{C}\delta_c$ value of
254 $-(47.2 \pm 5.8)\text{‰}$ inferred at R^2 above 0.4 is characteristic for the $\delta^{13}\text{C}$ of methane in the UT/LMS.
255 It is noteworthy that we have accounted for the biases in the analysed C1 WAS $\delta^{13}\text{C}(\text{CO})$ ex-
256 pected from the mass-independent isotope composition of O_3 (see details in Appendix B).

257 [18] We derive the “best-guess” estimate of the admixed CO ${}^{18}\text{O}$ signature at ${}^{18}\text{O}\delta_c =$
258 $+(92.0 \pm 8.3)\text{‰}$, which agrees with the other MM results obtained at R^2 above 0.75. Taking the
259 same subsets of samples, the concomitant ${}^{13}\text{C}$ signature matches ${}^{13}\text{C}\delta_c = -(23.3 \pm 8.6)\text{‰}$, indeed
260 at the upper end of the expected LMS $\delta^{13}\text{C}(\text{CO})$ variations of $-(25-31)\text{‰}$, which likely does
261 not allow the MM to ascertain this result as pertaining to the contamination (the corresponding
262 R^2 values are below 0.1). Upon the correction using the inferred ${}^{18}\text{O}\delta_c$ value, the C1 WAS
263 $\delta^{18}\text{O}(\text{CO})$ data appear adequate (shown with red symbols in Fig. 2). That is, variations in the
264 observed C^{18}O are driven by (i) the seasonal/regional changes in the composition of tropo-
265 spheric air and by (ii) the degree of mixing or replacement of the latter with the stratospheric
266 component that is less variable in ${}^{18}\text{O}$. This is seen as stretching of the scattered tropospheric
267 values ($[\text{CO}]$ above 60 nmol/mol) in a mixing fashion towards $\delta^{18}\text{O}(\text{CO})$ of around -10‰ at

268 [CO] of ~25 nmol/mol, respectively. The corrected C1 $\delta^{13}\text{C}(\text{CO})$ data (shown in Supplementary
269 Material, Fig. S4) are found to be in a $\pm 1\%$ agreement with the observations by B96, except for
270 several deep stratospheric samples ([CO] below 40 nmol/mol). The latter were encountered dur-
271 ing "ozone hole" conditions and carried extremely low ^{13}C abundances, which was attributed
272 to the reaction of methane with available free Cl radicals (Brenninkmeijer *et al.*, 1996).

3.2 Estimate of $\delta^{18}\text{O}(\text{O}_3)$

273 [19] The $^{18}\text{O}\delta_c$ signature inferred here ($^{18}\text{O}\delta_c = +(92.0 \pm 8.3)\%$) unambiguously pertains to O_3 and is
274 comparable to $\delta^{18}\text{O}(\text{O}_3)$ values measured in the stratosphere at temperatures about 30K lower
275 than those encountered in the UT/LMS by C1 (see Table 1 for comparison). If no other factors
276 are involved (see below), this discrepancy in $\delta^{18}\text{O}(\text{O}_3)$ should be attributed to the local condi-
277 tions, *i.e.* the higher pressures (typically 240–270 hPa for C1 cruising altitudes) at which O_3
278 was formed. Indeed, the molecular lifetime (the period through which the species' isotope reser-
279 voir becomes entirely renewed, as opposed to the "bulk" lifetime) of O_3 encountered along the
280 C1 flight routes is estimated on the order of minutes to hours at daylight (H. Riede, MPI-C,
281 2010), thus the isotope composition of the photochemically regenerated O_3 resets quickly ac-
282 cording to the local conditions. Virtual absence of sinks, in turn, leads to "freezing" of the
283 $\delta^{18}\text{O}(\text{O}_3)$ value during night in the UT/LMS. Verifying the current $\delta^{18}\text{O}(\text{O}_3)$ estimate against the
284 kinetic data, in contrast to the stratospheric cases, is problematic. The laboratory studies on O_3
285 formation to date have scrutinised the concomitant kinetic isotope effects (KIEs) as a function
286 of temperature at only low pressures (50 Torr); the attenuation of the KIEs with increasing pres-
287 sure was studied only at room temperatures (see Table 1, also Brenninkmeijer *et al.* (2003) for
288 references). A rather crude attempt may be undertaken by conjecturing an inhibition of the for-
289 mation KIEs proportional to that measured at ~320K, however applied to the nominal low-
290 pressure values reckoned at (220–230)K. A decrease in $\delta^{18}\text{O}(\text{O}_3)$ of about (5.9–7.6)% is ex-
291 pected from such calculation, yet accounting for a mere one-half of the (13.3–14.6)% "missing"
292 in $^{18}\text{O}\delta_c$.

293 [20] Lower $^{18}\text{O}\delta_c$ values could result from possible isotope fractionation accompanying the pro-
294 duction of the artefact CO. Although not quantifiable here, oxygen KIEs in the $\text{O}_3 \rightarrow \text{CO}$ con-
295 version chain cannot be ruled out, recalling that the intermediate reaction steps are not identifi-
296 able and the artefact CO represents at most 4% of all O_3 molecules. Furthermore, the yield λ_{O_3}
297 of CO from O_3 may be lower than unity (see details in Appendix A). On the other hand, the in-
298 ference that the contamination strength primarily depends on $[\text{O}_3]$ indicates that the kinetic frac-

299 tionation may have greater effect on the carbon isotope ratios of the artefact CO produced (the
300 ^{13}C δ_c values) in contrast to the oxygen ones. That is because all reactive oxygen available from
301 O_3 becomes converted to CO, whilst the concomitant carbon atoms are drawn from a virtually
302 unlimited pool whose apparent isotope composition is altered by the magnitude of the ^{13}C KIEs.

303 [21] Besides KIEs, selectivity in the transfer of O atoms from O_3 to CO affects the resulting ^{18}O δ_c
304 value. The terminal O atoms in O_3 are enriched w.r.t. to the molecular (bulk) O_3 composition
305 when the latter is above $\sim +70\%$ in $\delta^{18}\text{O}$ (Janssen, 2005; Bhattacharya *et al.*, 2008), therefore an
306 incorporation of only central O atoms into the artefact CO molecules should result in a reduced
307 apparent ^{18}O δ_c value. Such exclusive selection is, however, less likely from the kinetic stand-
308 point and was not observed in available laboratory studies (see Savarino *et al.* (2008) for a re-
309 view). For instance, Röckmann *et al.* (1998a) established the evidence of direct O transfer from
310 O_3 to the CO produced in alkene ozonolysis. A reanalysis of their results (in light of findings of
311 Bhattacharya *et al.* (2008)) suggests that usually the terminal atoms of the O_3 molecule become
312 transferred (their ratio over the central ones changes from the bulk $\sim 2:1$ to $\sim 1:0$ for various spe-
313 cies). Considering the alternatives of the O transfer in our case (listed additionally in Table 1),
314 the equiprobable incorporation of the terminal and central O_3 atoms into CO should result in the
315 $\delta^{18}\text{O}(\text{O}_3)$ value in agreement with the “crude” estimate based on laboratory data given above.

316 [22] Furthermore, the conditions that supported the reaction of O_3 (or its derivatives) followed by
317 the production of CO are vague. A few hypotheses ought to be scrutinised here. First, a fast
318 $\text{O}_3 \rightarrow \text{CO}$ conversion must have occurred, owing to short (*i.e.*, fraction of a second) exposure
319 time of the probed air to the contamination. Accounting for the typical C1 air sampling condi-
320 tions (these are: sampled air pressure of 240–270 hPa and temperature of 220–235K outboard
321 to 275–300K inboard, sampling rate of $\sim 12.85 \cdot 10^{-3}$ moles s^{-1} corresponding to 350L STP sam-
322 pled in 1200 s, inlet/tubing volume gauged to yield exposure times of 0.01 to 0.1 s due to vari-
323 able air intake rate, $[\text{O}_3]$ of 600 nmol/mol), the overall reaction rate coefficient (k_c in Eq. (A1)
324 from Appendix A) must be on the order of $6 \cdot 10^{-15} / \tau_c$ [$\text{molec}^{-1} \text{cm}^3 \text{s}^{-1}$], where τ_c is the exposure
325 time. Assuming the case of a gas-phase CO production from a recombining O_3 derivative and
326 an unknown carbonaceous compound X, the reaction rate coefficient for the latter ($^X k_r$ in
327 Eq. (A1) in Appendix A) must be rather high, at least $\sim 6 \cdot 10^{-10}$ [$\text{molec}^{-1} \text{cm}^3 \text{s}^{-1}$] over $\tau_c =$
328 $1/100$ s. This number decreases proportionally with growing τ_c and $[\text{X}]$, if we take less strict ex-
329 posure conditions. Nonetheless, in order to provide the amounts of artefact CO we detect, a
330 minimum abundance of 20 nmol/mol (or up to 4 μg of C per flight) of X is required, which is
331 not available in the UT/LMS from the species readily undergoing ozonolysis, *e.g.* alkenes.

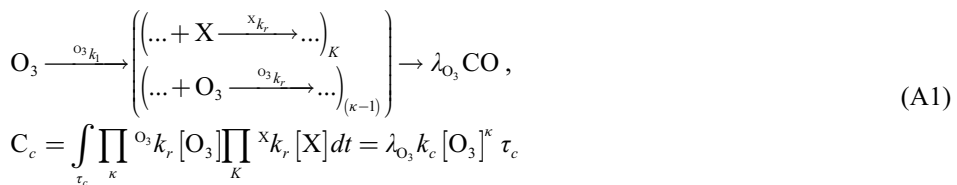
332 [23] Second, a more complex heterogeneous chemistry on the inner surface of the inlet or sup-
 333 plying tubing may be involved. Such can be the tracers' surface adsorption, (catalytic) decom-
 334 position of O₃ and its reaction with organics or with surface carbon that also may lead to the
 335 production of CO (Oyama, 2000). Evidence exists for the dissociative adsorption of O₃ on the
 336 surfaces with subsequent production of the reactive atomic oxygen species (see, *e.g.*,
 337 Li *et al.*, 1998, also Oyama, 2000). It is probable that sufficient amounts of organics have re-
 338 mained on the walls of the sampling line exposed to highly polluted tropospheric air, to be later
 339 broken down by the products of the heterogeneous decomposition of the ample stratospheric O₃.
 340 Unfortunately, the scope for a detailed quantification of intricate surface effects in the C1 CO
 341 contamination problem is very limited.

342 4 Conclusions

343 [24] Recapitulating, the *in situ* measurements of CO and O₃ allowed us to unambiguously quan-
 344 tify the artefact CO production from O₃ likely in the sample line of the CARIBIC-1 instrumen-
 345 tation. Strong evidence to that is provided by the isotope CO measurements. We demonstrate
 346 the ability of the simple mixing model ("Keeling-plot" approach) to single out the contamina-
 347 tion isotope signatures even in the case of a large sampling-induced mixing of the air with very
 348 different compositions. Obtained as a collateral result, the estimate of the δ¹⁸O(O₃) in the UT/
 349 LMS appears adequate, calling, however, for additional laboratory data (*e.g.*, the temperature-
 350 driven variations of the O₃ formation KIE at pressures above 100 hPa) for a more unambiguous
 351 verification.

352 Appendix A. Contamination kinetic framework

353 [25] We infer the O₃-exclusive functional dependence of the contamination strength C_c by dis-
 354 criminating the C1 outliers from respective C2 data in the following kinetic framework:



355 where k_c denotes the overall pseudo-first-order rate coefficient of the reaction chain leading to
 356 the artefact CO production with the respective yield λ_{O_3} . The individual rate coefficients ${}^X k_r$ and

357 $^{16}\text{O}_3k_r$ pertain to the unknown compound(s) X and O_3 reacting with the integral stoichiometry fac-
 358 tors K and κ , respectively. Practically we find that variations in C_c are exhaustively described
 359 using $[\text{O}_3]$, κ and k_c (the latter are obtained in a regression analysis). The value of k_c thus inte-
 360 grates the influence of the unknown (and likely invariable) $[X]$, $^{16}\text{O}_3k_r$ and K . The relation defined
 361 by Eq. (A1) provides the best approximation for C_c as a function of $[\text{O}_3]$ at $\kappa = 2.06 \pm 0.38$, sug-
 362 gesting two chain steps involving O_3 or its derivatives. At $\kappa = 2$, the ratio $C_c/[\text{O}_3]^2$ (essentially
 363 proportional to the reaction time τ_c and overall rate coefficient k_c) is found to be
 364 $(5.19 \pm 0.12) \cdot 10^{-5}$ mol/nmol ($\pm 1\sigma$, adj. $R^2 = 0.83$, red. $\chi^2 = 4.0$). The low uncertainty (within
 365 $\pm 3\%$) of this estimate signifies an exclusive dependence of the contamination source on the O_3
 366 abundance, as well as much similar reaction times τ_c . It is possible to constrain the overall yield
 367 λ_{O_3} of CO molecules in the artefact source chain to be between 0.5 and 1, comparing the magni-
 368 tude of C_c to the discrepancy between the $[\text{O}_3]$ measured in C1 and C2 (± 20 nmol/mol, taken
 369 equal to the $[\text{O}_3]$ bin size owing to the $\text{N}_2\text{O}-\text{O}_3$ and $\text{H}_2\text{O}-\text{O}_3$ distributions matching well be-
 370 tween the datasets). Lower λ_{O_3} values, otherwise, should have resulted in a noticeable (*i.e.*,
 371 greater than 20 nmol/mol) decrease in the C1 O_3 abundances with respect to the C2 levels.

372 **Appendix B. Corrections to measured $\delta^{13}\text{C}(\text{CO})$ values due to the oxygen**

373 **MIF**

374 [26] Atmospheric O_3 carries an anomalous isotope composition (or mass-independent fractiona-
 375 tion, MIF) with a substantially higher relative enrichment in ^{17}O over that in ^{18}O (above +25‰
 376 in $\Delta^{17}\text{O} = (\delta^{17}\text{O}+1)/(\delta^{18}\text{O}+1)^\beta - 1$, $\beta = 0.528$) when compared to the majority of terrestrial oxy-
 377 gen reservoirs that are mass-dependently fractionated (*i.e.*, with $\Delta^{17}\text{O}$ of $\sim 0\%$) (see Brennink-
 378 meijer *et al.* (2003) and refs. therein). CO itself also has an unusual oxygen isotopic composi-
 379 tion, possessing a moderate tropospheric MIF of around +5‰ in $\Delta^{17}\text{O}(\text{CO})$ induced by the sink
 380 KIEs in reaction of CO with OH (Röckmann *et al.*, 1998b; Röckmann *et al.*, 2002) and a minor
 381 source effect from the ozonolysis of alkenes (Röckmann *et al.*, 1998a; Gromov *et al.*, 2010). A
 382 substantial contamination of CO by O_3 oxygen induces proportional changes to $\Delta^{17}\text{O}(\text{CO})$ that
 383 largely exceed its natural atmospheric variation. Furthermore, the MIF has implications in the
 384 analytical determination of $\delta^{13}\text{C}(\text{CO})$, because the presence of C^{17}O species interferes with the
 385 mass-spectrometric measurement of the abundances of ^{13}CO possessing the same basic molecu-
 386 lar mass (m/e is 45). When inferring the exact $\text{C}^{17}\text{O}/\text{C}^{18}\text{O}$ ratio in the analysed sample is not
 387 possible, analytical techniques usually involve assumptions (*e.g.*, mass-dependently fractionated
 388 compositions or a certain non-zero $\Delta^{17}\text{O}$ value) with respect to the C^{17}O abundances

389 (Assonov and Brenninkmeijer, 2001). In effect for the C1 CO data, the artefact CO produced
 390 from O₃ had contributed with unexpectedly high C¹⁷O abundances that led to the overestimated
 391 δ¹³C(CO) analysed. Knowing the contamination magnitude C_c and assuming the typical O₃ MIF
 392 composition being ¹⁷OΔ_c, the respective bias ¹³Cδ_b is calculated using

$$\begin{cases} \Delta^{17}\text{O}(\text{CO}) \cong \left({}^{17}\text{O}\Delta_t C_t + {}^{17}\text{O}\Delta_c C_c \right) (C_a)^{-1} \\ {}^{13}\text{C}\delta_b = 7.2568 \cdot 10^{-2} \Delta^{17}\text{O}(\text{CO}) \end{cases}, \quad (\text{B1})$$

393 where ¹⁷OΔ_t denotes the natural, *i.e.* expected “true” value of Δ¹⁷O(CO). The remaining parame-
 394 ters pertain to the contamination kinetic framework (see Appendix A, Eq. (A1)). For the pur-
 395 pose of the current estimate it is sufficient to take ¹⁷Δ_n of +5‰ representing equilibrium en-
 396 richments expected in the remote free troposphere and UT/LMS. For the O₃ MIF signature ¹⁷Δ_c,
 397 the value of +30‰ (the average Δ¹⁷O(O₃) expected from the kinetic laboratory data at condi-
 398 tions met along the C1 flight routes, see Sect. 3.2 and Table 1) is adopted. The coefficient that
 399 proportionates ¹³Cδ_b and Δ¹⁷O in Eq. (B1) is reckoned for the CO with initially unaccounted MIF
 400 (*e.g.*, the sample is assumed to be mass-dependently fractionated) and quantifies some extra
 401 +0.73‰ in the analysed δ¹³C(CO) per every +10‰ of Δ¹⁷O(CO) excess (Assonov and
 402 Brenninkmeijer, 2001). The most contaminated C1 WAS CO samples at [O₃] above
 403 300 nmol/mol are estimated to bear Δ¹⁷O(CO) of (6–12)‰ corresponding to fractions of
 404 (0.10–0.27) of the artefact CO in the sample. Accordingly, the reckoned δ¹³C(CO) biases span
 405 (0.5–0.9)‰. Although not large, these well exceed the δ¹³C(CO) measurement precision of
 406 ±0.1‰ and were corrected for, and therefore are taken into account in the calculations with the
 407 MM presented in Sect. 3.1.

408 **Acknowledgements**

409 [27] The authors are indebted to Claus Koeppel, Dieter Scharffe and Dr. Andreas Zahn for their
 410 work and expertise on the carbon monoxide and ozone measurements in C1 and C2. Hella
 411 Riede is acknowledged for comprehensive estimates of the species lifetimes along the
 412 CARIBIC flight routes. We are grateful to Dr. Taku Umezawa, Dr. Angela K. Baker,
 413 Dr. Emma C. Leedham and ACP reviewers for the helpful discussions and comments on the
 414 manuscript.

415 **References**

- 416 Assonov, S. S. and Brenninkmeijer, C. A. M.: A new method to determine the ^{17}O isotopic abundance in
417 CO_2 using oxygen isotope exchange with a solid oxide, *Rapid Commun. Mass Spectrom.*, **15**, 2426–
418 2437, doi: [10.1002/rcm.529](https://doi.org/10.1002/rcm.529), 2001.
- 419 Assonov, S. S. and Brenninkmeijer, C. A. M.: A redetermination of absolute values for $^{17}\text{R}_{\text{VPDB-CO}_2}$ and
420 $^{17}\text{R}_{\text{VSMOW}}$, *Rapid Commun. Mass Spectrom.*, **17**, 1017–1029, doi: [10.1002/Rcm.1011](https://doi.org/10.1002/Rcm.1011), 2003.
- 421 Assonov, S. S., Brenninkmeijer, C. A. M., Koeppl, C., and Röckmann, T.: CO_2 isotope analyses using
422 large air samples collected on intercontinental flights by the CARIBIC Boeing 767,
423 *Rapid Commun. Mass Spectrom.*, **23**, 822–830, doi: [10.1002/rcm.3946](https://doi.org/10.1002/rcm.3946), 2009.
- 424 Bhattacharya, S. K., Pandey, A., and Savarino, J.: Determination of intramolecular isotope distribution of
425 ozone by oxidation reaction with silver metal, *J. Geophys. Res. Atm.*, **113**, D03303,
426 doi: [10.1029/2006jd008309](https://doi.org/10.1029/2006jd008309), 2008.
- 427 Brenninkmeijer, C. A. M.: Measurement of the abundance of ^{14}CO in the atmosphere and the $^{13}\text{C}/^{12}\text{C}$ and
428 $^{18}\text{O}/^{16}\text{O}$ ratio of atmospheric CO with applications in New Zealand and
429 Antarctica, *J. Geophys. Res. Atm.*, **98**, 10595–10614, doi: [10.1029/93JD00587](https://doi.org/10.1029/93JD00587), 1993.
- 430 Brenninkmeijer, C. A. M., Müller, R., Crutzen, P. J., Lowe, D. C., Manning, M. R., Sparks, R. J., and van
431 Velthoven, P. F. J.: A large ^{13}CO deficit in the lower Antarctic stratosphere due to “Ozone Hole”
432 Chemistry: Part I, Observations, *Geophys. Res. Lett.*, **23**, 2125–2128, doi: [10.1029/96gl01471](https://doi.org/10.1029/96gl01471), 1996.
- 433 Brenninkmeijer, C. A. M. and Röckmann, T.: Principal factors determining the $^{18}\text{O}/^{16}\text{O}$ ratio of
434 atmospheric CO as derived from observations in the southern hemispheric troposphere and lowermost
435 stratosphere, *J. Geophys. Res. Atm.*, **102**, 25477–25485, doi: [10.1029/97JD02291](https://doi.org/10.1029/97JD02291), 1997.
- 436 Brenninkmeijer, C. A. M., Crutzen, P. J., Fischer, H., Gusten, H., Hans, W., Heinrich, G.,
437 Heintzenberg, J., Hermann, M., Immelmann, T., Kersting, D., Maiss, M., Nolle, M., Pitscheider, A.,
438 Pohlkamp, H., Scharffe, D., Specht, K., and Wiedensohler, A.: CARIBIC – Civil aircraft for global
439 measurement of trace gases and aerosols in the tropopause region, *J. Atmos. Oceanic Technol.*, **16**,
440 1373–1383, doi: [10.1175/1520-0426\(1999\)016<1373:Ccafgm>2.0.Co;2](https://doi.org/10.1175/1520-0426(1999)016<1373:Ccafgm>2.0.Co;2), 1999.
- 441 Brenninkmeijer, C. A. M., Koeppl, C., Röckmann, T., Scharffe, D. S., Bräunlich, M., and Gros, V.:
442 Absolute measurement of the abundance of atmospheric carbon monoxide, *J. Geophys. Res. Atm.*, **106**,
443 10003–10010, doi: [10.1029/2000jd900342](https://doi.org/10.1029/2000jd900342), 2001.
- 444 Brenninkmeijer, C. A. M., Janssen, C., Kaiser, J., Röckmann, T., Rhee, T. S., and Assonov, S. S.: Isotope
445 effects in the chemistry of atmospheric trace compounds, *Chem. Rev.*, **103**, 5125–5161,
446 doi: [10.1021/Cr020644k](https://doi.org/10.1021/Cr020644k), 2003.

447 Brenninkmeijer, C. A. M., Crutzen, P., Boumard, F., Dauer, T., Dix, B., Ebinghaus, R., Filippi, D.,
448 Fischer, H., Franke, H., Frieß, U., Heintzenberg, J., Helleis, F., Hermann, M., Kock, H. H.,
449 Koepfel, C., Lelieveld, J., Leuenberger, M., Martinsson, B. G., Miemczyk, S., Moret, H. P.,
450 Nguyen, H. N., Nyfeler, P., Oram, D., O'Sullivan, D., Penkett, S., Platt, U., Pupek, M., Ramonet, M.,
451 Randa, B., Reichelt, M., Rhee, T. S., Rohwer, J., Rosenfeld, K., Scharffe, D., Schlager, H.,
452 Schumann, U., Slemr, F., Sprung, D., Stock, P., Thaler, R., Valentino, F., van Velthoven, P.,
453 Waibel, A., Wandel, A., Waschitschek, K., Wiedensohler, A., Xueref-Remy, I., Zahn, A.,
454 Zech, U., and Ziereis, H.: Civil Aircraft for the regular investigation of the atmosphere based on an
455 instrumented container: The new CARIBIC system, *Atmos. Chem. Phys.*, **7**, 4953–4976,
456 doi: [10.5194/acp-7-4953-2007](https://doi.org/10.5194/acp-7-4953-2007), 2007.

457 Coplen, T. B.: Reporting of stable hydrogen, carbon, and oxygen isotopic abundances (Technical Report),
458 *Pure Appl. Chem.*, **66**, 273–276, doi: [10.1351/pac199466020273](https://doi.org/10.1351/pac199466020273), 1994.

459 Craig, H.: Isotopic standards for carbon and oxygen and correction factors for mass-spectrometric analysis
460 of carbon dioxide, *Geochim. Cosmochim. Acta*, **12**, 133–149, doi: [10.1016/0016-7037\(57\)90024-8](https://doi.org/10.1016/0016-7037(57)90024-8),
461 1957.

462 Gonfiantini, R.: Standards for Stable Isotope Measurements in Natural Compounds, *Nature*, **271**, 534–536,
463 1978.

464 Gromov, S., Jöckel, P., Sander, R., and Brenninkmeijer, C. A. M.: A kinetic chemistry tagging technique
465 and its application to modelling the stable isotopic composition of atmospheric trace gases,
466 *Geosci. Model Dev.*, **3**, 337–364, doi: [10.5194/gmd-3-337-2010](https://doi.org/10.5194/gmd-3-337-2010), 2010.

467 Guenther, J., Erbacher, B., Krankowsky, D., and Mauersberger, K.: Pressure dependence of two relative
468 ozone formation rate coefficients, *Chem. Phys. Lett.*, **306**, 209–213,
469 doi: [10.1016/S0009-2614\(99\)00469-8](https://doi.org/10.1016/S0009-2614(99)00469-8), 1999.

470 Janssen, C., Guenther, J., Krankowsky, D., and Mauersberger, K.: Temperature dependence of ozone rate
471 coefficients and isotopologue fractionation in ^{16}O – ^{18}O oxygen mixtures, *Chem. Phys. Lett.*, **367**, 34–
472 38, doi: [10.1016/S0009-2614\(02\)01665-2](https://doi.org/10.1016/S0009-2614(02)01665-2), 2003.

473 Janssen, C.: Intramolecular isotope distribution in heavy ozone ($^{16}\text{O}^{18}\text{O}^{16}\text{O}$ and $^{16}\text{O}^{16}\text{O}^{18}\text{O}$),
474 *J. Geophys. Res. Atm.*, **110**, D08308, doi: [10.1029/2004jd005479](https://doi.org/10.1029/2004jd005479), 2005.

475 Johnston, J. C. and Thiemens, M. H.: The isotopic composition of tropospheric ozone in three
476 environments, *J. Geophys. Res. Atm.*, **102**, 25395–25404, doi: [10.1029/97jd02075](https://doi.org/10.1029/97jd02075), 1997.

477 Krankowsky, D., Bartecki, F., Klees, G. G., Mauersberger, K., Schellenbach, K., and Stehr, J.:
478 Measurement of heavy isotope enrichment in tropospheric ozone, *Geophys. Res. Lett.*, **22**, 1713–1716,
479 doi: [10.1029/95gl01436](https://doi.org/10.1029/95gl01436), 1995.

480 Krankowsky, D., Lämmerzahl, P., Mauersberger, K., Janssen, C., Tuzson, B., and Röckmann, T.:
481 Stratospheric ozone isotope fractionations derived from collected samples, *J. Geophys. Res. Atm.*, **112**,
482 D08301, doi: [10.1029/2006jd007855](https://doi.org/10.1029/2006jd007855), 2007.

483 Li, W., Gibbs, G. V., and Oyama, S. T.: Mechanism of Ozone Decomposition on a Manganese Oxide
484 Catalyst. 1. In Situ Raman Spectroscopy and Ab Initio Molecular Orbital
485 Calculations, *J. Am. Chem. Soc.*, **120**, 9041–9046, doi: [10.1021/ja981441+](https://doi.org/10.1021/ja981441+), 1998.

486 Mauersberger, K.: Measurement of Heavy Ozone in the Stratosphere, *Geophys. Res. Lett.*, **8**, 935–937,
487 doi: [10.1029/G1008i008p00935](https://doi.org/10.1029/G1008i008p00935), 1981.

488 Natrella, M.: NIST/SEMATECH e-Handbook of Statistical Methods, edited by: Croarkin, C. and
489 Tobias, P., NIST/SEMATECH, <http://www.itl.nist.gov/div898/handbook/> (last access: 07 May 2014),
490 2003.

491 Novelli, P. C., Masarie, K. A., and Lang, P. M.: Distributions and recent changes of carbon monoxide in
492 the lower troposphere, *J. Geophys. Res.*, **103**, 19015–19033, doi: [10.1029/98jd01366](https://doi.org/10.1029/98jd01366), 1998.

493 Novelli, P. C., Masarie, K. A., Lang, P. M., Hall, B. D., Myers, R. C., and Elkins, J. W.: Reanalysis of
494 tropospheric CO trends: Effects of the 1997–1998 wildfires, *J. Geophys. Res.*, **108**, 4464,
495 doi: [10.1029/2002jd003031](https://doi.org/10.1029/2002jd003031), 2003.

496 Oyama, S. T.: Chemical and Catalytic Properties of Ozone, *Catal. Rev. Sci. Eng.*, **42**, 279–322,
497 doi: [10.1081/cr-100100263](https://doi.org/10.1081/cr-100100263), 2000.

498 Pan, L. L., Randel, W. J., Gary, B. L., Mahoney, M. J., and Hints, E. J.: Definitions and sharpness of the
499 extratropical tropopause: A trace gas perspective, *J. Geophys. Res. Atm.*, **109**, D23103,
500 doi: [10.1029/2004jd004982](https://doi.org/10.1029/2004jd004982), 2004.

501 Röckmann, T., Brenninkmeijer, C. A. M., Neeb, P., and Crutzen, P. J.: Ozonolysis of nonmethane
502 hydrocarbons as a source of the observed mass independent oxygen isotope enrichment in tropospheric
503 CO, *J. Geophys. Res. Atm.*, **103**, 1463–1470, doi: [10.1029/97JD02929](https://doi.org/10.1029/97JD02929), 1998a.

504 Röckmann, T., Brenninkmeijer, C. A. M., Saueressig, G., Bergamaschi, P., Crowley, J. N.,
505 Fischer, H., and Crutzen, P. J.: Mass-independent oxygen isotope fractionation in atmospheric CO as a
506 result of the reaction CO+OH, *Science*, **281**, 544–546, doi: [10.1126/science.281.5376.544](https://doi.org/10.1126/science.281.5376.544), 1998b.

507 Röckmann, T., Jöckel, P., Gros, V., Bräunlich, M., Possnert, G., and Brenninkmeijer, C. A. M.: Using ¹⁴C,
508 ¹³C, ¹⁸O and ¹⁷O isotopic variations to provide insights into the high northern latitude surface CO
509 inventory, *Atmos. Chem. Phys.*, **2**, 147–159, doi: [10.5194/acp-2-147-2002](https://doi.org/10.5194/acp-2-147-2002), 2002.

510 Savarino, J., Bhattacharya, S. K., Morin, S., Baroni, M., and Doussin, J. F.: The NO+O₃ reaction: A triple
511 oxygen isotope perspective on the reaction dynamics and atmospheric implications for the transfer of
512 the ozone isotope anomaly, *J. Chem. Phys.*, **128**, 194303, doi: [10.1063/1.2917581](https://doi.org/10.1063/1.2917581), 2008.

513 Savarino, J. and Morin, S.: The N, O, S Isotopes of Oxy-Anions in Ice Cores and Polar Environments, in:
514 Handbook of Environmental Isotope Geochemistry, edited by: Baskaran, M., Advances in Isotope
515 Geochemistry, Springer Berlin Heidelberg, 835–864, 2012.

516 Scharffe, D., Slemr, F., Brenninkmeijer, C. A. M., and Zahn, A.: Carbon monoxide measurements onboard
517 the CARIBIC passenger aircraft using UV resonance fluorescence, *Atmos. Meas. Tech.*, **5**, 1753–1760,
518 doi: [10.5194/amt-5-1753-2012](https://doi.org/10.5194/amt-5-1753-2012), 2012.

519 Schinke, R., Grebenshchikov, S. Y., Ivanov, M. V., and Fleurat-Lessard, P.: Dynamical Studies Of The
520 Ozone Isotope Effect: A Status Report, *Annu. Rev. Phys. Chem.*, **57**, 625–661,
521 doi: [10.1146/annurev.physchem.57.032905.104542](https://doi.org/10.1146/annurev.physchem.57.032905.104542), 2006.

522 Stevens, C. M., Kaplan, L., Gorse, R., Durkee, S., Compton, M., Cohen, S., and Bielling, K.: The Kinetic
523 Isotope Effect for Carbon and Oxygen in the Reaction CO+OH, *Int. J. Chem. Kinet.*, **12**, 935–948,
524 doi: [10.1002/kin.550121205](https://doi.org/10.1002/kin.550121205), 1980.

525 Vicars, W. C., Bhattacharya, S. K., Erbland, J., and Savarino, J.: Measurement of the ¹⁷O-excess ($\Delta^{17}\text{O}$) of
526 tropospheric ozone using a nitrite-coated filter, *Rapid Commun. Mass Spectrom.*, **26**, 1219–1231,
527 doi: [10.1002/rcm.6218](https://doi.org/10.1002/rcm.6218), 2012.

528 Vicars, W. C. and Savarino, J.: Quantitative constraints on the ¹⁷O-excess ($\Delta^{17}\text{O}$) signature of surface
529 ozone: Ambient measurements from 50°N to 50°S using the nitrite-coated filter technique,
530 *Geochim. Cosmochim. Acta*, **135**, 270–287, doi: [10.1016/j.gca.2014.03.023](https://doi.org/10.1016/j.gca.2014.03.023), 2014.

531 Zahn, A., Brenninkmeijer, C. A. M., Maiss, M., Scharffe, D. H., Crutzen, P. J., Hermann, M.,
532 Heintzenberg, J., Wiedensohler, A., Güsten, H., Heinrich, G., Fischer, H., Cuijpers, J. W. M., and van
533 Velthoven, P. F. J.: Identification of extratropical two-way troposphere-stratosphere mixing based on
534 CARIBIC measurements of O₃, CO, and ultrafine particles, *J. Geophys. Res.*, **105**, 1527–1535,
535 doi: [10.1029/1999jd900759](https://doi.org/10.1029/1999jd900759), 2000.

536 Zahn, A., Brenninkmeijer, C. A. M., Asman, W. A. H., Crutzen, P. J., Heinrich, G., Fischer, H.,
537 Cuijpers, J. W. M., and van Velthoven, P. F. J.: Budgets of O₃ and CO in the upper troposphere:
538 CARIBIC passenger aircraft results 1997–2001, *J. Geophys. Res. Atm.*, **107**, 4337,
539 doi: [10.1029/2001jd001529](https://doi.org/10.1029/2001jd001529), 2002.

540 Zahn, A., Weppner, J., Widmann, H., Schlote-Holubek, K., Burger, B., Kühner, T., and Franke, H.: A fast
541 and precise chemiluminescence ozone detector for eddy flux and airborne application,
542 *Atmos. Meas. Tech.*, **5**, 363–375, doi: [10.5194/amt-5-363-2012](https://doi.org/10.5194/amt-5-363-2012), 2012.

544 Table 1. Ozone $^{18}\text{O}/^{16}\text{O}$ isotope ratios from literature and this study

Domain	T [K]	P [hPa]	$\delta^{18}\text{O}(\text{O}_3)$ [‰]	Remarks
Stratosphere	190–210	13–50	83–93 (<3)	1
UT/LMS	220–235	240–270	89–95 (8)	2
			84–88 (6)	T
			91–98 (9)	TC
			112–124 (17)	C
Laboratory	190–210	~67	87–97 (6)	3
	220–235	~67	102–110 (6)	3
	220–235	240–270	95–103	4

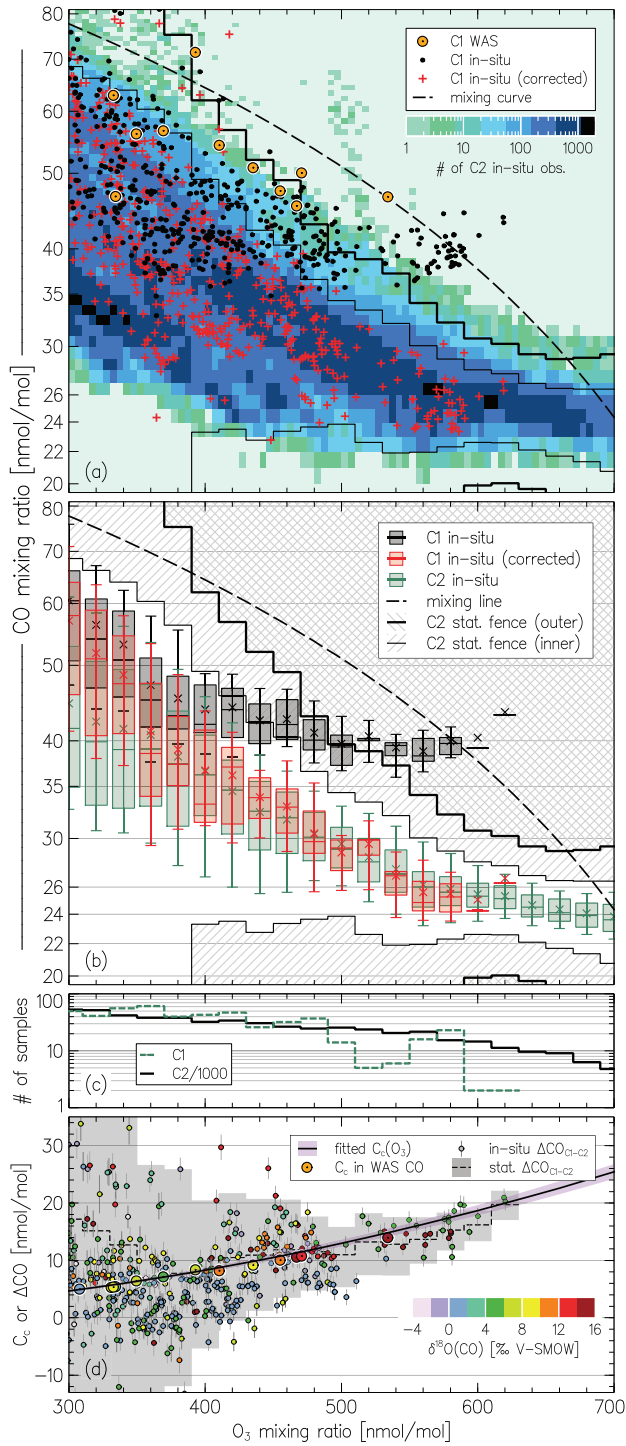
Notes: Values in parentheses denote the average of the estimates' standard errors. The expected O_3 isotope composition on the V-SMOW scale is calculated from the O_3 enrichments ε reported relative to O_2 using $\delta^{18}\text{O}(\text{O}_3)_{\text{V-SMOW}} = \delta^{18}\text{O}(\text{O}_2)_{\text{V-SMOW}} + {}^{18}\text{O}\varepsilon(\text{O}_3)_{\text{O}_2} + [\delta^{18}\text{O}(\text{O}_2)_{\text{V-SMOW}} \times {}^{18}\text{O}\varepsilon(\text{O}_3)_{\text{O}_2}]$.

¹ Observations (see Krankowsky *et al.* (2007) and refs. therein), lowermost values (19–25 km). Quoted temperature range is derived by matching measured $\delta^{18}\text{O}(\text{O}_3)$ and laboratory data (see note ³).

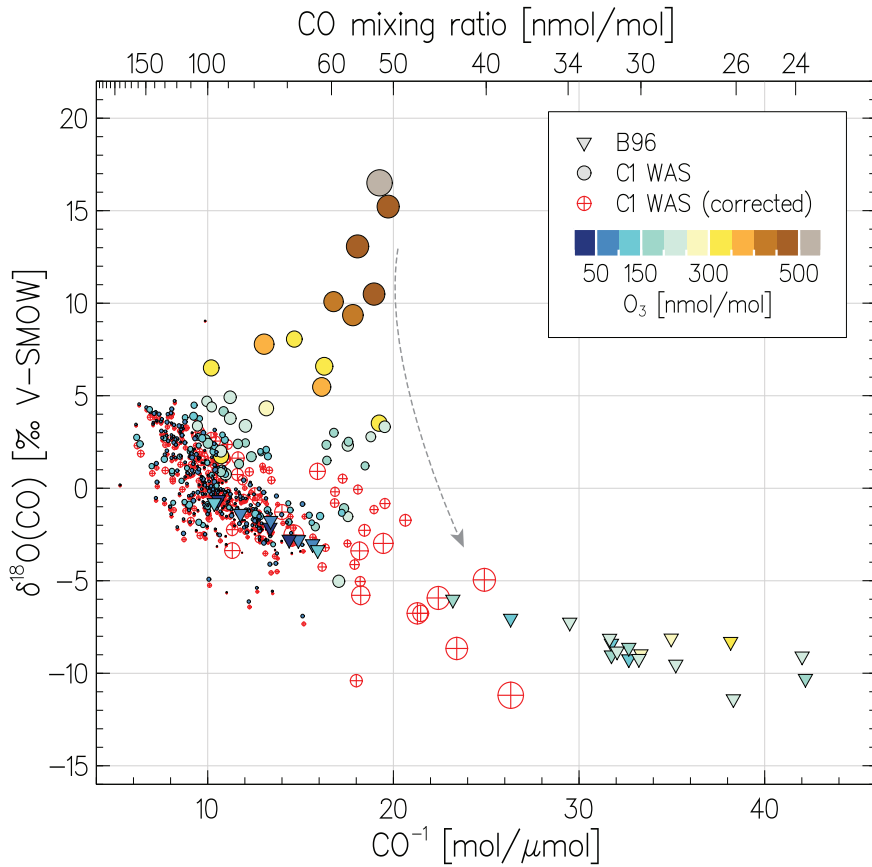
² This study, C1 observations (10–12 km). Letters denote the estimates derived using the data from Bhattacharya *et al.* (2008) and assuming only terminal (T), only central (C) and equiprobable terminal and central (TC) O_3 atoms transfer to the artefact CO .

³ Calculated using the laboratory KIE temperature dependence data summarised by Janssen *et al.* (2003).

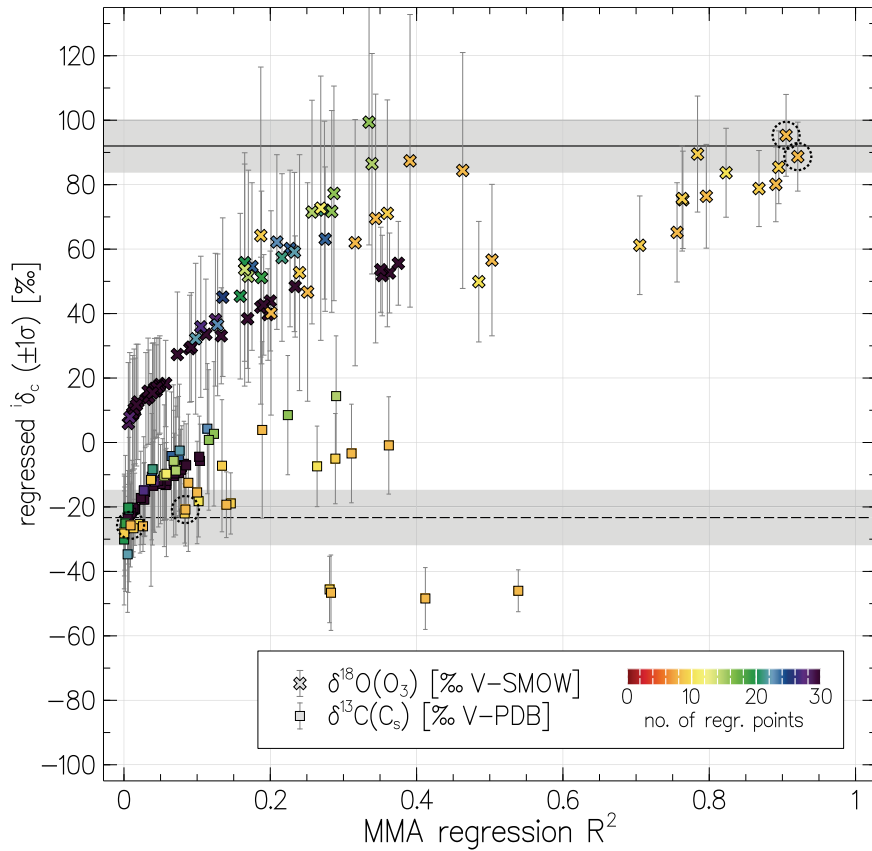
⁴ Calculated assuming a pressure dependence of the O_3 formation KIE similar to that measured at 320K (see Guenther *et al.* (1999) and refs. therein).



546 Fig. 1. (a) Distribution of CO mixing ratios as a function of concomitant O₃ mixing ratios measured by
547 CARIBIC in the LMS ([O₃]>300 nmol/mol). The shaded area is the two-dimensional histogram of the C2
548 measurements (all C2 data obtained until June 2013) counted in 5×1 nmol/mol size [O₃]×[CO] bins, thus
549 darker areas emphasise greater numbers of particular CO–O₃ pairs observed. Small symbols denote the
550 original C1 *in situ* measurements (black) and corrected for the artefacts (red); the C1 WAS analyses (11 of
551 total 408) are shown with large symbols. Thin and thick step-lines demark the inner and outer statistical
552 fences (ranges outside which the data points are considered mild or extreme outliers, see text) of the C2
553 data, respectively. The dashed curve exemplifies compositions expected from the linear mixing of very
554 different (*e.g.*, tropospheric and stratospheric) end-members. (b) Statistics on CO mixing ratios from C1
555 and C2 data shown in box-and-whisker diagrams for samples clustered in 20 nmol/mol O₃ bins (whiskers
556 represent 9th/91st percentiles). (c) Sample statistic for each CARIBIC dataset (note the C2 figures scaled
557 down by a factor of 1000). (d) Estimates of the C1 *in situ* CO contamination strength C_c as a function of
558 [O₃] (solid line) obtained by fitting the difference ΔCO between the C2 and C1 *in situ* [CO] (small sym-
559 bols) in the kinetic framework (see Appendix A, Eq. (A1)). Step line shows the ΔCO for the statistical av-
560 erages (the shaded area equals the height of the inner statistical fences of the C2 data). Large symbols de-
561 note the estimates of C_c in the C1 WAS data (slight variations *vs.* the *in situ* data are due to the sample
562 mixing effects, see Sect. 3). Colour denotes the respective C1 WAS $\delta^{18}\text{O}(\text{CO})$ (note that typically 6–7
563 *in situ* measurements correspond to one WAS sample). Note: The entire C1 CO/O₃ dataset is presented in
564 the Supplementary Material, Fig. S1.



565 Fig. 2. ¹⁸O/¹⁶O isotope composition of CO as a function of its reciprocal mixing ratio. Triangles present
 566 the data from the remote SH UT/LMS obtained by Brenninkmeijer *et al.* (1996) (B96). Colour refers to the
 567 concomitantly observed O₃ abundances; note the extremely low [O₃] encountered by B96 in the Antarctic
 568 "ozone hole" conditions. Filled and hollow circles denote the original and corrected (as exemplified by the
 569 dashed arrow) C1 WAS data, respectively, with the symbol size scaling proportional to the estimated con-
 570 tamination magnitude (see text).



571 Fig. 3. Results of the regression calculation with the MM. Shown with symbols are the contamination
 572 source isotope signatures $i\delta_c$ as a function of the respective coefficient of determination (R^2). Colour denotes
 573 the number of samples in each subset selected. Solid and dashed lines present the best guess ± 1 SD
 574 for the $\delta^{18}\text{O}(\text{O}_3)$ and $\delta^{13}\text{C}(\text{C}_g)$ estimates. Dashed circles mark the values obtained at highest R^2 for $^{18}\text{O}\delta_i$ re-
 575 gression (above 0.9). See text for details.